ACS APPLIED MATERIALS & INTERFACES

www.acsami.org

Research Article

Cascade Enzymes Confined in DNA Nanoanchors for Antitumor Therapy

Danyu Wang,[†] Xin Zhou,[†] Mengyu Huang, Jie Duan, Yue Qiu, Hua Yi, Yang Wang, Huimin Xue, Jiali Zhang, Qiuxia Yang, Hua Gao,* Zhenzhen Guo,* and Kaixiang Zhang*

Cite This: *ACS Appl. Mater. Interfaces* 2024, 16, 50295−50304

Read Online

ACCESS | Metrics & More | Article Recommendations | Supporting Information

ABSTRACT: Cascade-enzyme reaction systems have emerged as promising tools for treating malignant tumors by efficiently converting nutrients into toxic substances. However, the challenges of poor localized retention capacity and utilization of highly active enzymes often result in extratumoral toxicity and reduced therapeutic efficacy. In this study, we introduced a cell membrane−DNA nanoanchor (DNANA) with a spatially confined cascade enzyme for in vivo tumor therapy. The DNANAs are constructed using a polyvalent cholesterol-labeled DNA triangular prism, ensuring high stability in cell membrane attachment. Glucose oxidase (GOx) and horseradish peroxidase (HRP), both modified with streptavidin, are precisely confined to biotin-labeled DNANAs. Upon intratumoral injection, DNANA enzymes efficiently colonize the tumor site through cellular membrane engineering strategies, significantly reducing off-target enzyme leakage and the associated risks of extratumoral toxicity. Furthermore, DNANA enzymes demonstrated effective cancer therapy in vitro and in vivo by depleting glucose and producing highly cytotoxic hydroxyl radicals in the vicinity of tumor cells. This membrane-engineered cascade-enzyme reaction system presents a conceptual approach to tumor treatment.

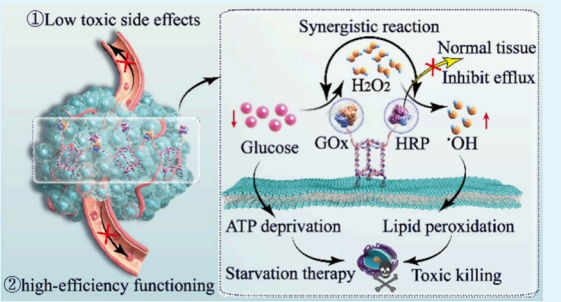

KEYWORDS: *cell membrane engineering, DNA nanostructure, catalytic nanomedicines, anticancer therapy, cascade reactions*

INTRODUCTION

Cascade-enzyme systems efficiently catalyze nutrient reactions, transforming the original substrates into highly potent antitumor agents. This catalytic efficiency enhances therapeutic outcomes, reduces the required therapeutic dosage for patients, and minimizes toxic side effects.[1−3] Additionally, the strategy can effectively tackle intricate challenges such as tumor heterogeneity and resistance to conventional chemotherapy drugs. Consequently, cascade-enzyme systems are increasingly being explored for cancer treatment.[4,5]

At present, most studies focus on loading proteins onto nanocarriers for systemic cancer therapy,[6−8] due to the challenges associated with therapeutic proteins, such as instability, high immunogenicity, poor tissue permeability, short circulation time, and severe side effects.[9−11] For instance, Sun et al. recently developed a liposome enzyme nanoreactor for antitumor treatments. The cocompartmentalization of two enzymes within the liposome created a confined microenvironment, increasing the local concentration of intermediate products and thereby enhancing the efficiency of the cascade reaction, effectively inhibiting both in vitro and in vivo tumor growth.[12] Other carriers for enzyme loading include hollow mesoporous silica, metal−organic frameworks, polymers, etc.[13−15] While these enzyme nanomaterials have shown good efficacy in cancer treatment, at least one of the following issues remains: (1) weak retention in local tumor sites and low utilization, (2) poor penetration capability in tumor tissues, (3) inadequate spatial distance restrictions between cascade enzymes, leading to reduced reaction rates, (4) requirement of prolonged traversal through the tumor barrier and the cell membrane barrier to enter the cell, and (5) the potential risk of high toxicity from the systemic administration of highly active enzymes.

Compared with systemic administration, local drug-delivery systems offer the advantage of direct drug delivery to tumor tissues, bypassing the bloodstream. This approach helps to evade the circulatory system, reducing systemic toxicity and minimizing drug degradation and inactivation, thereby enhancing the therapeutic efficacy against solid tumors.[16−18] Additionally, local drug delivery resolves the challenges that may prevent surgical intervention due to the tumor type, stage, location, or patient health status. While the current tumor treatment based on in situ administration has enhanced safety, small molecules, proteins, and other nanomedicines still tend to diffuse from the tumor site to nearby normal tissues, causing

Received: June 13, 2024
Revised: August 26, 2024
Accepted: September 1, 2024
Published: September 12, 2024

certain potential side effects. To address this issue, the current effective drug retention strategy primarily relies on the utilization of massive polymers such as hydrogels[19−21] and microneedles.[22,23] However, these methods have some drawbacks such as the cumbersome process of in situ administration, prolonged drug-release times, and insufficient contact between protein enzymes and substrates. The most significant concern is that drugs released from large polymeric carriers can still diffuse from the tumor into adjacent normal tissues because they lack the ability to stay localized at the tumor site. Therefore, there is an urgent need for strategies to localize protein enzymes within tumors without large polymer encapsulation for safer and more effective treatment.

Cell membrane surface engineering is a technology that attaches substances to the cell membrane surface. The current methods of cell membrane surface engineering include genetic engineering,[24−26] chemical cross-linking,[27,28] ligand binding,[29−33] and hydrophobic insertion.[34−38] Among these, hydrophobic insertion has been widely used in cell sensing and cell therapy due to its rapidity, simplicity, and universal connection and the characteristic of high abundance attachment of cross-linking substances to the cell membrane. However, the application of protein-based cell membrane engineering in disease treatment has rarely been reported.

In the study, we developed a cell membrane−DNA nanoanchor (DNANA) with a spatially restricted protein cascade enzyme for antitumor therapy (Figure 1). The multivalent cholesterol-labeled DNA triangular prism nanoanchor is designed to persistently reside at the tumor site through a stable cell membrane engineering strategy.[39] When the enzyme is connected to the DNANA through an avidin−biotin linkage, efficient retention of the enzyme at the tumor site is achieved, inhibiting its diffusion from the tumor site to normal tissues, significantly enhancing enzyme utilization. Glucose oxidase (GOx) catalyzes the depletion of glucose nutrients in the vicinity of tumor cells, concurrently generating a high concentration of hydrogen peroxide (H_2O_2) in situ to facilitate the second-stage reaction of horseradish peroxidase (HRP). The HRP further converts H_2O_2 to highly cytotoxic hydroxyl radicals, which kills tumor cells. Due to the spatial confinement provided by DNANA, the transport efficiency of intermediate metabolites between cascade enzymes is improved. The DNANA enzymes showed good biocompatibility and efficient antitumor efficacy in vitro and in vivo.

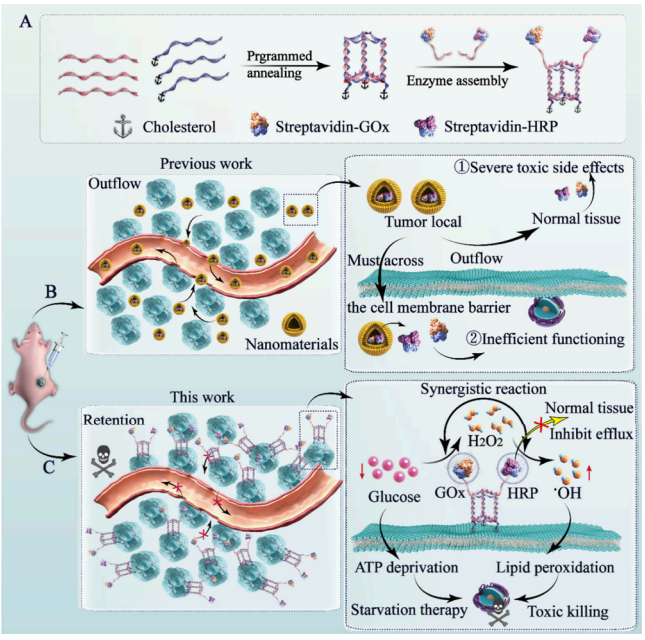

Figure 1. (A) Schematic representation of the assembly process for DNANA enzymes. (B) Illustration depicting the typical diffusion of nanoenzymes from tumors in previous studies. (C) Working schematic showing the enhanced local retention of nanoenzymes within tumors using DNANA-enzyme-engineered cell membranes, along with their proposed antitumor mechanism.

RESULTS AND DISCUSSION

Preparation of an Engineered Cell Membrane Cascade Reaction System. The amphiphilic DNANA framework structure, designed for cell membrane engineering, was synthesized as depicted in Figure 2A and Table S1. The synthesis was achieved through PCR-programmed annealing, and the resulting products were characterized by using agarose gel electrophoresis, as shown in Figure 2B. As the number of DNA strands involved in the assembly of the DNANA increased, a corresponding delay in the migration of gel bands was observed. Specifically, lane 3 represents the DNANA main framework structure, while lanes 4 and 5 depict the DNANA loaded with one and two biotin-labeled arm strands, respectively. Lane 7 showcases DNANA that contains three

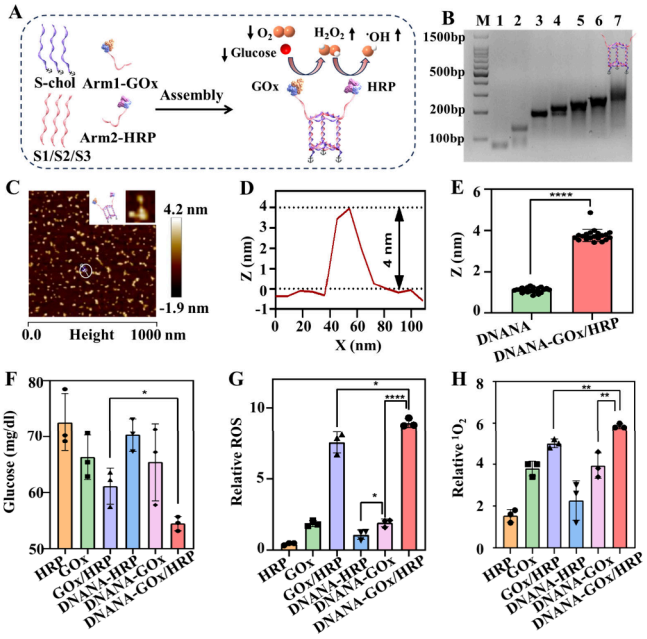

Figure 2. Construction and catalytic performance evaluation of the DNANA enzymes. (A) Schematic of the DNANA-GOx/HRP assembly protocol. (B) Agarose gel characterization of the DNANA assembly. From line 1 to line 7: DNA marker, S1, S1 + S2, S1 + S2 + S3, S1 + S2 + S3 + arm 1, S1 + S2 + S3 + arm 1 + arm 2, S1 + S2 + S3 + arm 1 + arm 2 + arm 3, and S1 + S2 + S3 + arm 1 + arm 2 + S-chol. (C) AFM imaging of DNANA-GOx/HRP. (D) Height analysis of DNANA-GOx/HRP using data sourced from part C. (E) Comparative height analysis of DNANA-GOx/HRP versus DNANA based on the AFM data. (F) Evaluation of the catalytic activity of DNANA enzymes in glucose consumption in solution. (G and H) Assessment of DNANA-enzyme-mediated ROS and $^1O_2$ production in solution.

https://doi.org/10.1021/acsami.4c09835
ACS Appl. Mater. Interfaces 2024, 16, 50295−50304

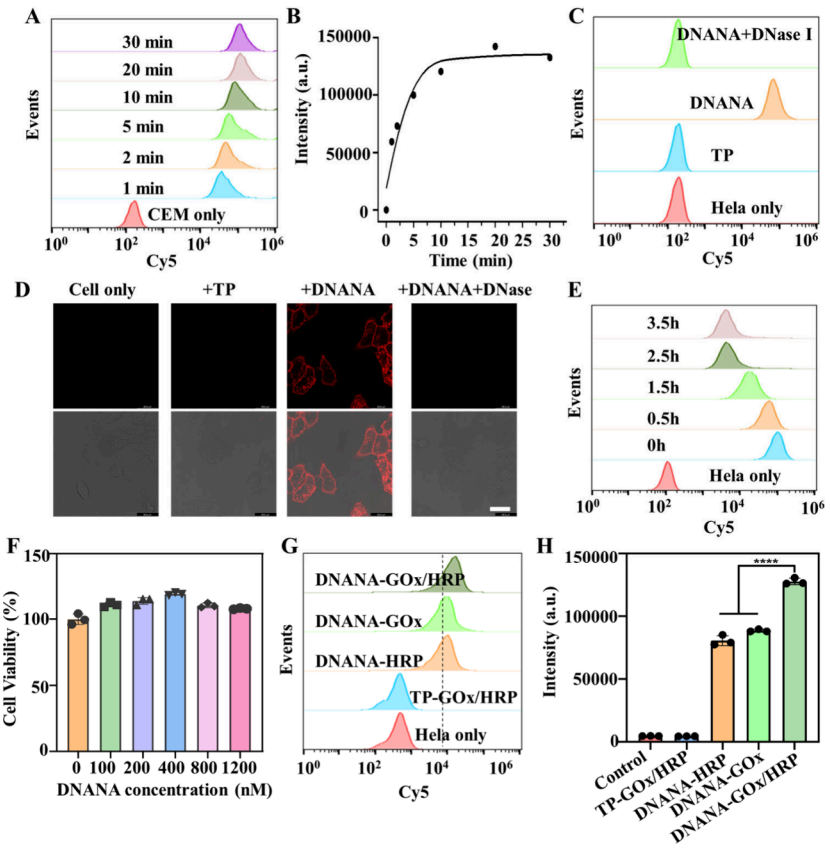

Figure 3. Anchoring of DNANA and DNANA-GOx/HRP to the cell membrane. (A) Flow cytometric characterization of DNANA anchored to cells at different time points. (B) Time-dependent curve analysis of DNANA anchoring on cells; data from part A. (C) Flow cytometric characterization of the nuclease-mediated degradation of DNANA on the HeLa cell membrane. (D) Confocal imaging of nuclease degradation of DNANA on the HeLa cell. Scale bar: 30 μm. (E) Stability of DNANA on the cell membrane at different times analyzed by flow cytometry in a medium containing 10% FBS at 37 °C. (F) Cytotoxicity evaluation of DNANA against a HeLa cell. (G) Flow cytometric analysis of DNANA enzymes anchored to HeLa cells. (H) Statistical analysis of significant differences in the flow cytometry results in part G (n = 3).

cholesterol-labeled DNA strands and two biotin-labeled arm strands. The successful connection between streptavidin (SA)-labeled GOx, HRP enzyme, and a biotin-labeled arm strand is also confirmed by polyacrylamide gel electrophoresis results (Figure S1). The progressively slower migration of DNANA, DNANA-GOx, and DNANA-GOx/HRP in agarose gel electrophoresis further indicates that the DNANA-enzyme complex has been successfully constructed (Figure S1). The morphologies of DNANA and DNANA-GOx/HRP were subsequently verified using atomic force microscopy (AFM), and the results are illustrated in Figures 2C and S2A. The measured heights of the two structures were approximately 1.3 and 4.0 nm, respectively (Figures 2D and S2B). Statistical analysis of the height differences of DNANA and DNANA-GOx/HRP confirms the successful enzyme attachment to the DNANA (Figure 2E). It is important to note that the 1.3 nm height measurement of the DNANA nanostructure by AFM can be influenced by several factors, potentially causing discrepancies between the theoretical and measured values. These factors include sample deformation due to tip−sample interactions, tip convolution effects, substrate effects, sample preparation methods, tip−sample adhesion, and calibration and instrumental limitations.[35,37]

Following this, the catalytic properties of the spatially restricted cascade-enzyme reaction system of DNANA were thoroughly investigated. The system was evaluated for its ability to catalyze reactions involving glucose consumption, oxygen radicals, and single-linear oxygen species production. The results, which are depicted in Figures 2F−H and S3, demonstrate that the DNANA-based confined cascade-enzyme reaction system exhibits a higher consumption of glucose and an increased production of reactive oxygen species (ROS) as well as singlet oxygen species. These findings indicate an enhancement in the efficiency of the cascade-enzyme reaction, which can be attributed to the engineered DNANA-based system. The contributing factors include the following: (a) The proximity between GOx and HRP facilitates the rapid transfer of intermediates, such as H_2O_2, from GOx to HRP, minimizing loss or degradation before reaching HRP (enhanced substrate channeling). (b) With decreasing distance between GOx and HRP, the time required for intermediates to travel is reduced, thereby accelerating the overall reaction rate. (c) Spatial confinement within the DNANA system elevates the local concentration of intermediates around HRP, enhancing catalytic turnover because HRP more frequently encounters substrate molecules.

Evaluation of the Cell Membrane Labeling Performance of DNANA. The ability to integrate DNANA labels into cell membranes in a straightforward, rapid, abundant, and stable manner is a crucial prerequisite for effectively localizing the cascade-enzyme reaction system at the cellular membrane site. To facilitate the evaluation of DNANA's membrane-labeling efficiency, Cy5 was conjugated to DNANA. Subsequently, the binding efficacy of DNANA with varying

https://doi.org/10.1021/acsami.4c09835
ACS Appl. Mater. Interfaces 2024, 16, 50295−50304

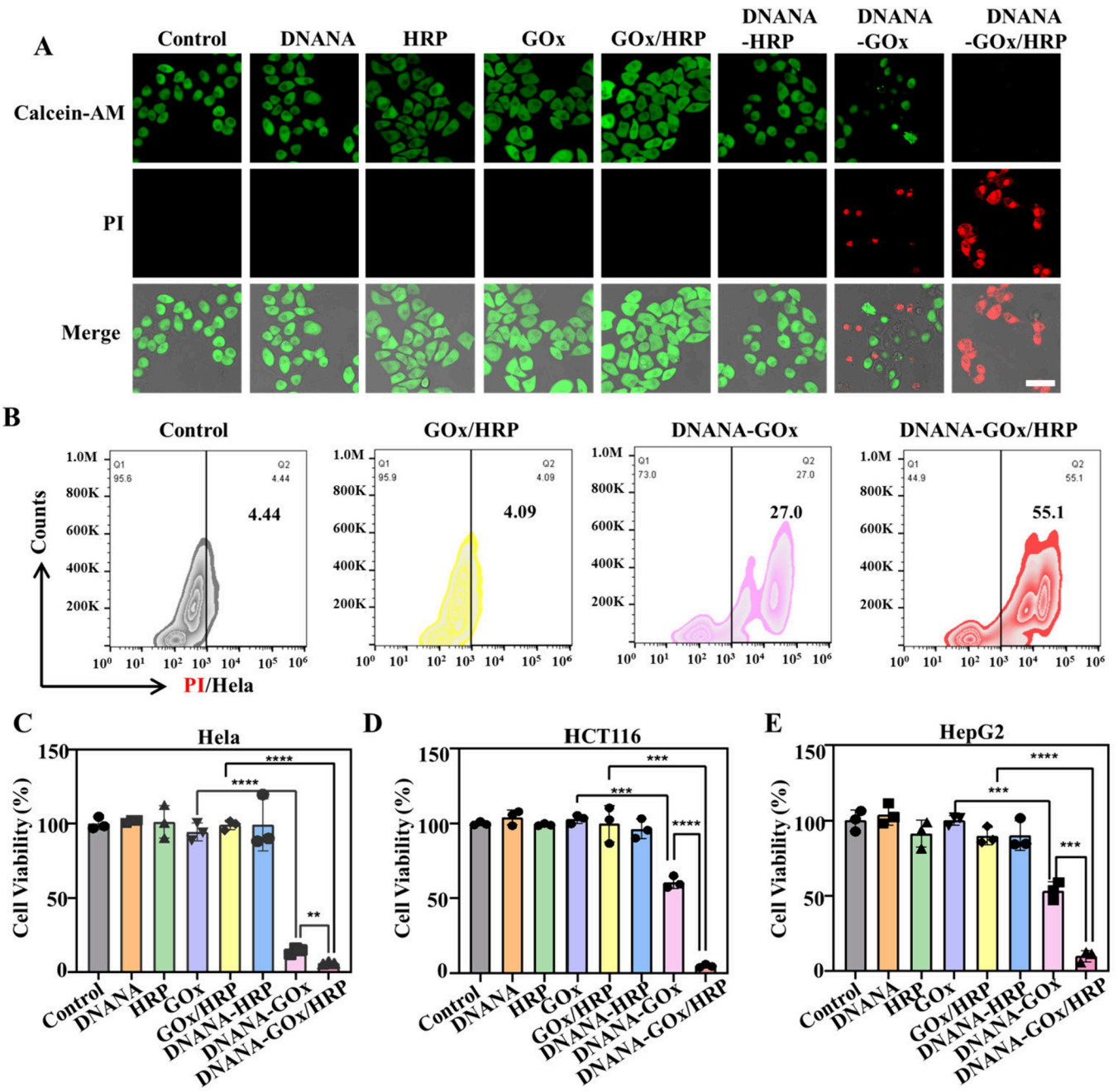

Figure 4. Cytotoxicity of DNANA enzymes against tumor cells in vitro. (A) Confocal imaging of HeLa cells treated with different groups and stained with Calcein-AM and PI. Scale bar: 50 μm. (B) Flow cytometric analysis of DNANA enzyme-induced cytotoxicity in HeLa cells. (C−E) Cytotoxicity assessment of DNANA enzymes against HeLa, HCT116, and HepG2 cells using CCK-8 assay.

cholesterol valencies was assessed using flow cytometry. The data presented in Figure S3 reveal a direct correlation between the augmented fluorescence intensity and increased cholesterol valency, indicating that trivalent DNANA has a greater affinity for cell membranes. Further experiments were conducted to determine the optimal time and concentration for labeling cell membranes with trivalent cholesterol−DNANA by flow cytometry. As shown in Figure 3A,B, the human acute lymphoblastic leukemia cells (CCRF-CEM) cell membranes exhibited pronounced fluorescent signals within 1 min of DNANA application, which plateaued at 10 min, suggesting a rapid anchoring process to the cell membrane. Flow cytometry analysis identified an effective DNANA labeling concentration on the outer CEM cell membrane as 200 nM (Figure S4). Similarly, the experiments ascertained that the HeLa cell reached an effective saturation concentration for DNANA labeling at 300 nM (Figure S5). These findings highlight the inherent variances in cell membrane architectures across different cell types. Additionally, when nucleases were introduced to the Cy5-DNANA-anchored HeLa cell samples, the fluorescence on the surface of HeLa cell membranes disappeared, consistent with the control group. This result indicates that DNANA is anchored on the outer side of the cell membrane (Figure 3C,D). The same conclusion was also confirmed in the CEM cells (Figure S6).

The stability of the attachment of DNANA to cell membranes was evaluated under conditions featuring 10% fetal bovine serum (FBS), which contained nucleases and

https://doi.org/10.1021/acsami.4c09835
ACS Appl. Mater. Interfaces 2024, 16, 50295−50304

cationic proteins. Flow cytometry analysis showed negligible changes in the fluorescence intensity after 2 h at 25 °C, demonstrating the constructs' resistance to the binding of complex cationic proteins (Figure S7). At 37 °C, a gradual decrease in the fluorescence intensity of Cy5 was observed, yet a pronounced fluorescence signal persisted past 3.5 h (Figure 3E). These findings underscore the anchoring stability of DNANA on the cellular membrane, primarily influenced by nucleolytic degradation, while also demonstrating DNANA's considerable resilience under challenging environmental conditions. Moreover, no cytotoxicity was detected even at concentrations up to 1200 nM, as verified by Cell Counting Kit-8 (CCK-8) assays, which underscores the excellent biocompatibility of the DNANA strategy (Figure 3F). Building upon these findings, Cy5-SA-GOx and Cy5-SA-GOx/HRP cascade enzymes were attached to DNANA, demonstrating the DNANA's capacity to confine cascade enzymes to the cell membrane surface, as depicted in Figures 3G,H and S8. Robust fluorescence signals in flow cytometry and marked discrepancies in histogram analyses substantiated the effective anchorage of DNANA-GOx, DNANA-HRP, and DNANA-GOx/HRP to cellular membranes. These experiments collectively indicate that DNANA exhibits outstanding properties for cell membrane engineering across various cell types and demonstrates an effective ability to immobilize proteins on the cell membrane surface.

Cell Cytotoxicity of the DNANA-Confined Cascade-Enzyme System. Building on the verified excellence of DNANA in cell membrane labeling and its proficiency in anchoring cascade enzymes, we expanded our research to evaluate the cytotoxic potential of DNANA-linked cascade enzymes against cancerous cells. The dose−response relationship of the antitumor activity of DNANA-GOx/HRP was quantitatively measured using CCK-8 assay, with the results presented in Figure S9. At a concentration threshold of 10 nM, a near-complete ablation of HeLa cells was observed, thereby establishing 10 nM as the optimal concentration for follow-up experimental investigations. The initial phase involved gauging the toxicity of DNANA cascade-enzyme constructs against HeLa cancer cells using a Calcein-AM/propidium iodide (PI) staining assay. Calcein-AM stained viable cells green, while PI stained dead cells red. The outcomes of confocal imaging, to be depicted in Figures 4A and S9, revealed that isolated enzymes (GOx, HRP, and the combination GOx/HRP) manifested strong green fluorescence coupled with faint red fluorescence, mirroring the blank control cell group with an over 98% cell survival. This suggests that free enzymes have minimal cytotoxic effects when they are not confined by DNANA.

In pronounced contrast, the DNANA-GOx and combined DNANA-GOx/HRP ensembles both showed a surge in red fluorescence alongside diminished green fluorescence, particularly in the latter group. These observations imply that the membrane-labeling and spatial-confinement capabilities provided by DNANA boost the cooperative cytotoxic effects of the enzymes upon tumor cells. Conversely, DNANA-HRP groups did not exhibit antitumor effects, likely due to the insufficient H_2O_2 levels in the cell medium required for the HRP enzyme to generate cytotoxic ROS (Figure S9). Flow cytometry analyses lent further support to the conclusion of DNANA-restricted enzymes exhibiting formidable antitumor efficacy (Figures 4B and S10). As indicated by the results, the cell survival rate of all enzyme groups without DNANA linkage and a DNANA-HRP group was consistent with that of control cells without any treatment, and the cell survival rate exceeding 95%. The survival rates of cells treated with DNANA-GOx and DNANA-GOx/HRP were only 73% and 45%. Additionally, using Calcein-AM/PI assay, the potent tumor-eliminating capabilities of the DNANA-enzyme system were also confirmed in CEM cancer cell models, as demonstrated in Figure S11.

CCK-8 assay was employed to appraise the cytotoxic effects of the DNANA−enzyme conjugates on HeLa cells, further confirming their lethality (Figure 4C). To evaluate the broader applicability of our designed cascade-enzyme-engineered membrane system for the eradication of cancer cells, we expanded our research to encompass the cytotoxicity of DNANA enzymes against HCT116, HepG2, and B16F10 cell lines using the CCK-8 methodology. As illustrated in Figures 4D,E and S12, all cellular toxicity assays disclosed that both DNANA-GOx and DNANA-GOx/HRP were proficient in extinguishing tumor cells, with the DNANA-GOx/HRP complex displaying enhanced efficacy in inducing tumor cell mortality. The empirical data presented above decisively verify the feasibility of our proposed cascade-enzyme-engineered cell membrane system for cancer therapy. The data, as illustrated in Figure 4C−E, clearly showed that cell survival rates surpassed 95% across all tested cell types in the presence of unbound enzymes, mirroring the outcomes observed in the phosphate-buffered saline (PBS) control group. This suggests that the enzymes, when not linked to a carrier, do not impart significant cytotoxic effects on these cell lines. In contrast, DNANA-GOx induced substantial cytotoxicity, causing approximately 80% mortality in HeLa cells, 60% in B16F10 cells, 50% in HepG2 cells, and 45% in HCT116 cells. This difference in susceptibility to DNANA-GOx treatment across various tumor cell types likely reflects their intrinsic cellular heterogeneity. Critically, the DNANA-GOx/HRP cascade-enzyme system achieved death rates exceeding 90% across all tested tumor cell lines. The results above demonstrate that our constructed DNANA-enzyme cascade-engineered cell membrane strategy possesses efficient and universal tumor-killing capabilities.

Study on the Mechanism of DNANA Killing Tumor Cells. The well-established principle underlying the cascade reaction of GOx and HRP enzymes involves glucose consumption, leading to the generation of H_2O_2 and ROS. This process can induce cell death through both nutrient deprivation and the cytotoxic effects of strong oxidizing agents. To further validate that our constructed DNANA enzymes retain this tumor-killing mechanism, we initially performed a glucose detection assay to assess glucose consumption. The results, as shown in Figure 5A, indicate a significant decrease in the glucose content in the DNANA-GOx and DNANA-GOx/HRP sample groups, with the latter exhibiting even lower glucose levels. This is attributed to the catalytic consumption of H_2O_2 by HRP, which, in turn, accelerates glucose depletion by GOx. No glucose consumption was observed in other sample groups, suggesting the crucial role of the enzyme−cell membrane connection in glucose consumption. The reduction in the glucose content subsequently led to a decrease in nicotinamide adenine dinucleotide (NADH) production, as shown in Figures 5B and S12. Given that NADH is a critical coenzyme for adenosine triphosphate generation, its reduction results in cellular starvation and eventual death due to insufficient energy supply.

https://doi.org/10.1021/acsami.4c09835
ACS Appl. Mater. Interfaces 2024, 16, 50295−50304

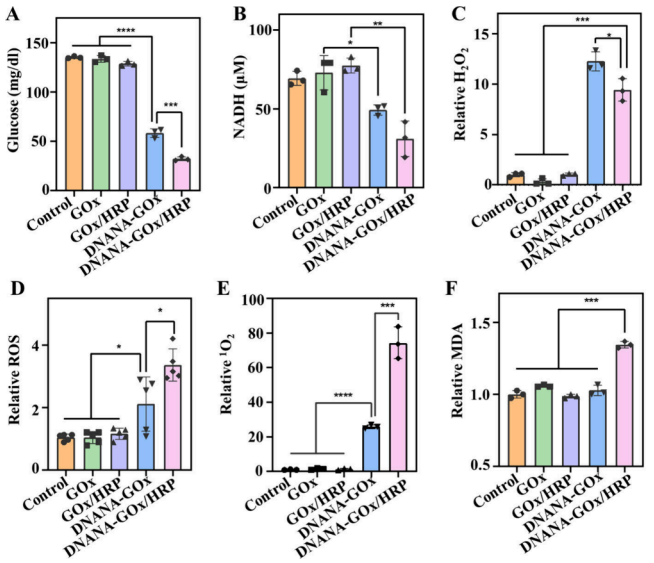

Figure 5. Mechanism of DNANA-enzyme-induced cytotoxicity in cancer cells. (A) Changes in the glucose concentration after treatment of HeLa cells with DNANA enzymes. (B) Changes in the NADH concentration after the treatment of HeLa cells with DNANA enzymes. (C) H_2O_2 production after the treatment of HeLa cells with DNANA enzymes. (D) Relative ROS levels measured by DCFH-DA after the treatment of HeLa cells with DNANA enzymes. (E) Relative $^1O_2$ levels measured by SOSG after the treatment of HeLa cells with DNANA enzymes. (F) Relative MDA levels measured by thiobarbituric acid assay after the treatment of HeLa cells with DNANA enzymes.

Subsequently, H_2O_2 levels were further investigated using a H_2O_2 detection kit, and the results in Figure 5C demonstrate an increase in the H_2O_2 content for both DNANA-GOx and DNANA-GOx/HRP, with the latter exhibiting lower H_2O_2 levels due to the additional consumption by the HRP-catalyzed reaction. In the second stage of the HRP reaction, the production of highly toxic ROS becomes a crucial mechanism for inducing cell death. ROS levels were evaluated using ROS detection kits, and the results in Figure 5D show elevated ROS levels for both DNANA-GOx and DNANA-GOx/HRP, with a particularly pronounced increase in the latter. This validates the efficient cascade reaction efficiency of DNANA-restricted cascade enzymes. Furthermore, we assessed the levels of active oxygen species, such as singlet oxygen, using a singlet oxygen detection kit (Figure 5E). The results further support our findings because active oxygen can induce oxidative stress and lipid peroxidation in tumor cells, leading to cell death. The detection of malondialdehyde (MDA), a byproduct of this process, is demonstrated in Figure 5F. The data collectively indicate that only the DNANA-enzyme sample group exhibits nutrient depletion and toxic substance production, highlighting the efficacy and underlying mechanism of the DNANA-engineered cascade-enzyme system in effectively destroying tumor cells.

In Vivo Assessment of the Therapeutic Efficacy. The high abundance and prolonged residence of DNANA labels within the tumor site are prerequisites for the safe in vivo treatment of tumors. Following in situ administration to the tumor (Figure 6A), the biodistribution of Cy5-DNANA over time was qualitatively assessed through in vivo imaging. As illustrated in Figure S13, Cy5-DNANA maintained a strong fluorescence intensity at the tumor site 24 h postadministration, whereas cholesterol-unmodified DNA exhibited complete fluorescence disappearance at 6 h. This suggests that the cholesterol-mediated cell membrane insertion strategy induces efficient retention of DNANA labels at the tumor site. Building upon this, enzymes modified with Cy5-SA were connected to DNANA, and their ability to cascade enzymes planted at the tumor site was further investigated through in vivo imaging. The results, as shown in Figure 6B, revealed that enzyme-coupled DNANA sustained strong fluorescence at the tumor site, with no significant decay even at 48 h. In contrast, the free Cy5-SA-modified enzyme control group exhibited the rapid decline in the fluorescence intensity over time, nearly

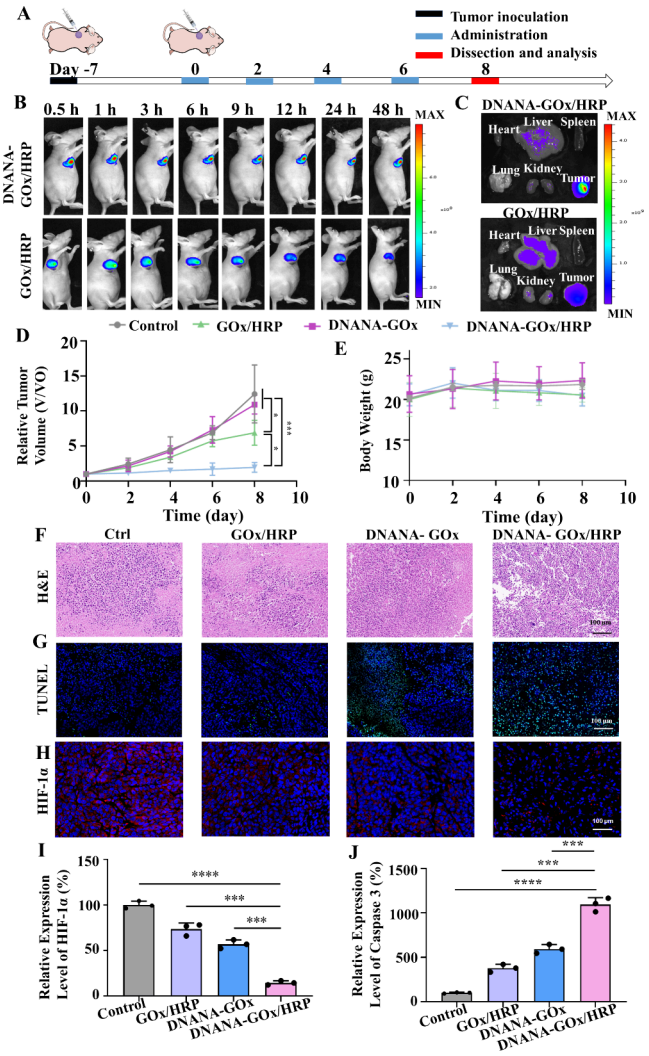

Figure 6. Evaluation of DNANA-GOx/HRP for in vivo antitumor therapy. (A) Animal administration protocol. (B) In vivo fluorescence imaging of mice at different time points after intratumoral injection of Cy5-GOx/Cy5-HRP and DNANA-Cy5-GOx/Cy5-HRP. (C) Ex vivo imaging of the major organs (heart, liver, spleen, lungs, and kidneys) and tumor in two groups of mice after 48 h. (D) Relative tumor volume of mice treated with saline, GOx/HRP, DNANA-GOx, and DNANA-GOx/HRP. (E) Changes in the body weight of mice after different treatments. (F and G) TUNEL and H&E staining of tumor tissues in different treatment groups. (H and I) Analysis of the HIF-1α relative expression and significant differences in tumor tissues of different treatment groups. (J) Analysis of the differences in the relative expression of Caspase 3 in tumor tissues of different treatment groups. Significant differences determined by the Student's t test were defined as $^*p < 0.05$ and $^{***}p < 0.001$.

https://doi.org/10.1021/acsami.4c09835
ACS Appl. Mater. Interfaces 2024, 16, 50295−50304

disappearing at 48 h. Further investigation involving imaging of the creatures' vital organs at 48 h, as indicated in Figure 6C, revealed that the DNANA−enzyme conjugates were predominantly retained within the tumors, with minimal dispersion into normal tissues and organs. Conversely, the unattached enzymes, while present at moderate levels in the tumor, were primarily detected in the liver and kidneys. This distribution pattern indicates that free enzymes can easily migrate from the tumor to normal tissues, posing a significant risk of toxic side effects in nontargeted areas. Collectively, the in vivo imaging insights from the murine model indicate that our fabricated DNANA is a highly effective method for confining enzyme-based drugs to tumor sites, presenting substantial promise for safe and effective cancer treatment.

In the conclusive phase of the study, the therapeutic efficacy of the DNANA-enzyme system in combating tumors was evaluated. Changes in the tumor volume over an 8-day period and the weights of tumors from various test groups are displayed in Figure 6D,E. Relative to the PBS and GOx/HRP groups, those treated with DNANA-GOx and DNANA-GOx/HRP exhibited significant suppression of tumor growth. Specifically, the DNANA-GOx/HRP combination exhibited a significantly stronger inhibitory effect on tumor progression. This observation implies that the strategic spatial arrangement of cascade enzymes can result in increased catalytic activity, thereby enhancing the therapeutic efficacy. The survival of all mice during the 8-day observation period is encouraging, suggesting that the treatments were well-tolerated. While there were natural variances in the body weight among the different groups, none exhibited substantial weight loss, further indicating the absence of severe systemic toxicity from the treatments administered (Figure 6E).

Furthermore, the posttherapeutic antitumor effects across the different test groups were evaluated using hematoxylin and eosin (H&E) staining, a standard method for examining tissue morphology (Figures 6F). The resulting images reveal that the tumors from the PBS control group and the group with unbound enzymes maintained histological characteristics consistent with aggressive growth including deeply stained nuclei, enlarged nuclear size, reduced cytoplasmic volume, and densely packed tumor cells. Conversely, the tumors from mice that received the DNANA-enzyme treatment displayed markedly different features, such as the shrinkage of tumor cells, the presence of necrotic tissue that stains uniformly red, and evidence of cellular separation. These morphological changes are indicative of cell apoptosis, signifying that the DNANA-enzyme therapy induced significant tumor necrosis. Additional examination of apoptotic cells was carried out through terminal deoxynucleotidyl transferase-mediated dUTP nick end labeling (TUNEL) staining, which specifically marks DNA fragmentation that occurs during apoptosis. As shown in Figure 6G, the DNANA-enzyme group exhibited more potent green fluorescence compared to the other groups, indicating higher apoptosis rates. Moreover, the tumor cell death phenomenon was more pronounced in the DNANA-GOx/HRP samples, demonstrating the heightened efficiency of the cell-membrane-engineered antitumor effect of spatially constrained cascade enzymes. These results are highly consistent with those of in vitro cell experiments.

In addition, we found that the cascade-enzyme system could alleviate the hypoxic state at the tumor site. HIF-1α, a characteristic indicator of the hypoxic environment, showed significantly weaker red fluorescence in the DNANA-GOx/HRP group than in the control group (Figure 6H,I). This may be due to the catalyzed intermediate H_2O_2 by HRP, which enhances the reaction efficiency of the cascade enzyme and further damages the tumor tissue. Similarly, analysis of the levels of the proliferation marker Ki67 and the apoptosis marker Caspase 3 in tumor tissues from each treatment group showed that the DNANA-GOx/HRP group efficiently inhibited tumor progression (Figures S14 and 6J). These results are highly consistent with in vitro cell experiments.

The safety assessment of the various treatments included comprehensive monitoring of changes in the complete blood count and the histology of normal organs following the administration of different samples to the mice. The data from Figure S15 indicate that the blood routine values for mice in all treated groups fell within the normal ranges, suggesting that no hematological toxicity was caused by the treatments. Furthermore, the toxicity of the various treatments was further evaluated through histological analysis of the major organs, including the heart, liver, spleen, lungs, and kidneys. The results indicated that none of the treatments caused any pathological damage or abnormalities in these organs across all groups (Figure S16). These findings demonstrate that DNANA-enzyme treatment offers excellent biocompatibility and safety profiles in the context of tumor therapy.

CONCLUSION

We developed a cell-membrane-anchored nanoreactor system that incorporates DNANA-conjugated cascade enzymes, tailored for enhanced catalytic antitumor therapy. The DNANA-conjugated cascade enzymes ensure sustained in vivo retention within tumors in mice while exhibiting negligible diffusion into normal tissues, thereby demonstrating exceptional biological safety. Furthermore, due to the spatial constraints imposed by DNANA on GOx and HRP, this further accelerates glucose consumption and the generation of ROS, thereby promoting efficient tumor therapy. Unlike approaches that retain protein enzymes in tumors by encapsulating them within large-scale materials such as hydrogels, our nanoscale strategy affords several benefits: it facilitates more straightforward drug delivery, increases the efficacy of catalytic functions, and boosts the efficiency of cascade-enzyme reactions. This development heralds a new paradigm in protein enzyme carrier systems for antitumor treatment and is set to stimulate further research into the safety and efficacy of catalytic drugs in tumor therapy.

EXPERIMENTAL PROCEDURES

Materials. All DNA oligonucleotides were obtained from Sango Biotech (China) and Hippo Biotech (China). Biotinylated GOx was purchased from Yucai Pharmaceuticals (China). Biotinylated HRP was obtained from Corehui Co., Ltd. (China). Streptavidin (SA) was purchased from Aladdin Biochemical Technology Co., Ltd. (China). The nucleic acid dye GelRed, Dulbecco's modified Eagle's medium (DMEM), Hoechst-33342, CCK-8 assay, and cell apoptosis detection kit were purchased from Solarbio Science and Technology Co., Ltd. (China). The serum used for the cell culture was purchased from LONSERA of Shuangru Biotech. Glucose detection kits, singlet oxygen green fluorescence probe, Calcein-AM/PI cell viability, and cytotoxicity detection kits were sourced from Beyotime Biotechnology Co., Ltd. (China). The hexokinase activity assay kit was obtained from Yakeyin Biotechnology Co., Ltd. (China). The hydrogen peroxide (H_2O_2) content assay kit and malondialdehyde (MDA) content assay kit were obtained from Solarbio Science and

https://doi.org/10.1021/acsami.4c09835
ACS Appl. Mater. Interfaces 2024, 16, 50295−50304

Technology Co., Ltd. (China). Shiyanjia Lab (www.shiyanjia.com) provided support for the atomic force microscope.

Preparation of DNANA-GOx/HRP. To synthesize DNANA, 1 μL of each of the three complementary 20 μM single-stranded (ss)DNAs (S1, S2, and S3) was used. The DNA strands were mixed and annealed using a PCR machine according to the following temperature program: 95 °C (5 min); 95−85 °C (−1 °C/min); 85−35 °C (−0.1 °C/min); 35−4 °C (−1 °C/min); 4 °C (forever). The reaction was conducted in a 1× reaction buffer (20 mM Tris, 12.5 mM magnesium chloride, 2 mM EDTA, pH 7.4), The resulting DNANA was then stored at 4 °C for subsequent experiments. Cholesterol was anchored to DNANA at room temperature by incubating the mixture for 1 h, resulting in the formation of amphiphilic DNANAs. A total of 10 μL of 20 μM DNANA was added to preincubated SA (20 μM) dissolved in phosphate-buffered saline (PBS), along with a mixture of biotin−ssDNA and GOx/HRP.

Native Polyacrylamide Gel Electrophoresis (Native-PAGE). A 10% natural polyacrylamide gel was prepared to characterize the successful ligation between the enzyme and nucleic acids. A total of 10 μL of a 0.5 μM DNA sample and 2 μL of a 6× loading buffer were mixed. Electrophoretic analysis was performed in a fresh 1× TAE electrophoresis buffer. Electrophoresis was carried out in an ice−water bath at 90 V for 15 min and then switched to 110 V for 60 min. Subsequently, the polyacrylamide gels were stained with GelRed for 30 min and then imaged and analyzed using a Tanon 2000 Gel Imaging System (China) and Image Lab software.

Agarose Gel Electrophoresis. A 3% agarose gel was prepared for native electrophoresis. A total of 10 μL of a DNA sample was mixed with 2 μL of a 6× loading buffer to create the sample solution. A 100-base-pair DNA ladder was used as a DNA molecular weight size marker. Electrophoresis was performed in a fresh 1× TAE electrophoresis buffer at 110 V. Subsequently, agarose gels were imaged and analyzed by using a Tanon 2000 gel imaging system.

Cell Culture. The cell lines used in this experiment include HeLa, CCRF-CEM (human acute lymphoblastic T lymphocytes), HepG2, HCT116, and B16F10. The HeLa, HepG2, HCT116, and B16F10 cells were cultured in fresh DMEM supplemented with 1% penicillin−streptomycin and 10% FBS at 37 °C in a humidified atmosphere with 5% CO_2. The CCRF-CEM cells were cultured in a fresh RPMI 1640 medium supplemented with 1% penicillin−streptomycin and 10% FBS at 37 °C in a humidified atmosphere with 5% CO_2 in a cell culture incubator.

Enzyme Digestion Experiment. To characterize the anchoring of DNANA on the outer surface of the cell membrane, incubation was carried out at 37 °C using a medium containing DNase I and DNase III (Thermo Fisher). Cy5-labeled DNANA was incubated with HeLa cells in a blank medium for 1 h at room temperature, followed by centrifugation and removal of the supernatant. Then, 2 μL of DNase I and 1 μL of DNase III were added to 100 μL of PBS, and the cells were incubated at 37 °C for 2 h. After washing twice with a PBS buffer, the enzyme digestion results were observed using a confocal microscope (LEICA TCS SP8 STED) and a flow cytometer (FongCyte, Challen Bio).

Stability of DNANA. The membrane anchoring stability of Cy5-labeled DNANA in a fresh culture medium containing 10% FBS was detected. Cy5-labeled DNANA with one, two, or three cholesterols was separately incubated with CCRF-CEM cells in a blank medium at room temperature for 1 h, followed by centrifugation and removal of the supernatant. Then, a fresh culture medium containing 10% FBS was added, and the samples were further incubated at room temperature for 2 h. After washing twice with PBS, analysis was performed using flow cytometry. During the process, samples were oscillated at a speed of 170 rpm, and approximately 10000 events were counted for each sample.

Cell Viability Assay. The cell cytotoxicity of DNANA, HRP, GOx, GOx/HRP, DNANA-HRP, DNANA-GOx, and DNANA-GOx/HRP against HeLa, HepG2, HCT116, and B16F10 cells was determined by using CCK-8 assay. HeLa, HepG2, HCT116, and B16F10 cells were seeded in 96-well plates at a density of 5×10^3 cells/well and incubated at 37 °C for 24 h. After the culture medium was removed, the cells were washed twice with PBS and then 50 μL of PBS containing the samples (where the concentration of DNANA was 300 nM and the concentration of the enzyme was 10 nM) was incubated per well for 1 h at 37 °C and 5% CO_2. Afterward PBS was removed, and 100 μL of a culture medium containing FBS was added to each well. After 24 h of further incubation, the culture medium was removed, and each well was washed twice with PBS. A fresh culture medium (100 μL/well) was added, followed by the addition of 10 μL of CCK-8 solution (MCE, USA) per well. The 96-well plate was then incubated in a cell culture incubator for half an hour and shaken for 1 min, and the absorbance at 450 nm was measured using a microplate reader. The calculation of the cell viability is as follows: cell viability = $(OD_{sample} - OD_{blank})/(OD_{control} - OD_{blank})$, where $OD_{control}$ and OD_{sample} represent the absorbance at 450 nm when the sample is absent and present, respectively. OD_{blank} represents the absorbance at 450 nm of wells without cells.

Live/Dead Cell Assay. Further staining with Calcein-AM and PI was performed to evaluate the in vitro antitumor efficacy. A staining solution was prepared by adding 2 μL of Calcein-AM solution and 2 μL of PI solution to 2 mL of PBS. HeLa and CCRF-CEM cells were seeded in confocal dishes at a density of 5×10^3 cells/well and incubated for 24 h. Subsequently, the cells were treated with DNANA, HRP, GOx, GOx/HRP, DNANA-HRP, DNANA-GOx, or DNANA-GOx/HRP (where the concentration of DNANA was 300 nM and the concentration of the enzyme was 10 nM). After 1 h of incubation in the culture chamber, PBS was removed, and DMEM containing FBS (200 μL/well) was added. After being incubated for 24 h, the cells were washed with a PBS buffer. Each well was stained with 200 μL of staining solution and incubated at 37 °C for 30 min. The supernatant was removed, and the cells were washed twice with a PBS buffer. Finally, images of the stained cells were obtained by using a confocal microscope (LEICA TCS SP8 STED).

Study on the Mechanism of DNANA Killing Tumor Cells. Detection of the glucose, H_2O_2, MDA, $^1O_2$, and ROS content changes in the culture medium after treatment of the cells with DNANA enzymes: HeLa cells were seeded at a density of 5000 cells/well in a 96-well plate and cultured in a fresh DMEM high glucose complete medium for 24 h at 37 °C and 5% CO_2 in a cell culture incubator. Afterward, the samples were added to the wells and allowed to react for 1 h. The reaction mixture was then aspirated, and the wells were washed twice with PBS before a fresh culture medium was added. Following 24 h of further incubation, the supernatant was removed and processed according to the glucose, H_2O_2, and MDA assay kit method, with the final absorbance values measured at 630, 415, 532, and 504 nm using a microplate reader.

In Vivo Imaging. Female BALB/c-nu mice, aged 5−6 weeks, were purchased from Sipeifu Biotechnology Co., Ltd. Approximately 1×10^6 HeLa cells were injected into the right axilla of each mouse to establish the tumor-bearing mouse model. A total of 100 μL of DNANA-GOx/HRP solution at a concentration of 200 nM (10 nM for GOx and HRP) or an equal dose of GOx/HRP was injected into via tail vein in the body of tumor-bearing mice. At predetermined time points postadministration (0.5, 1, 3, 6, 9, 12, 24, and 48 h), the mice were anesthetized and imaged using the NightOWL 206 II LB983 in vivo imaging system (Berthold Technologies). After being photographed, the mice were euthanized, and the tumors and five major organs (heart, liver, spleen, lungs, and kidneys) were dissected for ex vivo imaging and analysis of the biodistribution of the GOx/HRP and DNANA-GOx/HRP groups. All experiments were conducted following the animal use and care regulations of the Henan Animal Experimental Center, China.

In Vivo Antitumor Therapy. Tumor models were constructed by subcutaneous injection of 200 μL of HeLa cell suspension (1×10^6 cells) into the right axilla of 5−6-week-old female BALB/c-nu mice. After the tumor volume grew to approximately 50 mm^3, the tumor-bearing mice were randomly divided into four groups ($n = 6$) and treated with 60 μL of PBS and GOx/HRP, DNANA-GOx, and DNANA-GOx/HRP (DNANA concentration of 200 nM and GOx/HRP concentration of 10 nM), respectively, for intratumor injection. The tumor volume and body weight of the mice were recorded every

https://doi.org/10.1021/acsami.4c09835
ACS Appl. Mater. Interfaces 2024, 16, 50295−50304

other day. At the end of treatment, blood samples were collected from mice in each group for a complete blood count. The mice were euthanized, and the tumors were dissected to prepare sections for H&E, TUNEL, and immunofluorescence staining. Sections of the major organs (heart, liver, spleen, lungs, and kidneys) were stained for H&E.

Statistical Analysis. All data in this paper were treated using a Student's *t* test, and statistical analyses were performed by *GraphPad* software. All of results were presented by mean ± standard deviation. *P* values: $*P < 0.05$, $**P < 0.01$, $***P < 0.001$, and $****P < 0.0001$.

■ ASSOCIATED CONTENT

Supporting Information

The Supporting Information is available free of charge at https://pubs.acs.org/doi/10.1021/acsami.4c09835.

Characterization of enzymes binding with DNANA, AFM imaging analysis, standard curve for glucose content detection, assessment of saturation concentrations, flow cytometry characterization and analysis, stability of DNANA, evaluation of DNANA enzymes killing HeLa cells, cytotoxic effects, evaluation of DNANA retention stability, imaging analysis of Ki67 and Caspase 3, complete blood count analysis, histological analysis of major organs, and oligonucleotide sequences utilized in the study (PDF)

■ AUTHOR INFORMATION

Corresponding Authors

Hua Gao − *School of Basic Medical Sciences, Zhengzhou University, Zhengzhou 450001, China*; Email: gaohua212@zzu.edu.cn

Zhenzhen Guo − *Henan Key Laboratory of Nanomedicine for Targeting Diagnosis and Treatment, School of Pharmaceutical Sciences, Zhengzhou University, Zhengzhou 450001, China*; orcid.org/0009-0003-1364-6628; Email: zhenzhenguo@zzu.edu.cn

Kaixiang Zhang − *Henan Key Laboratory of Nanomedicine for Targeting Diagnosis and Treatment, School of Pharmaceutical Sciences, Zhengzhou University, Zhengzhou 450001, China; Tianjian Laboratory of Advanced Biomedical Sciences, Zhengzhou University, Henan 450001, China; State Key Laboratory of Esophageal Cancer Prevention and Treatment, Zhengzhou University, Zhengzhou 450052, China*; orcid.org/0000-0002-6812-6342; Email: zhangkx@zzu.edu.cn

Authors

Danyu Wang − *Henan Key Laboratory of Nanomedicine for Targeting Diagnosis and Treatment, School of Pharmaceutical Sciences, Zhengzhou University, Zhengzhou 450001, China*; orcid.org/0000-0002-3127-5328

Xin Zhou − *Institute of Biomedical Engineering, College of Life Sciences, Qingdao University, Qingdao 266071, China*

Mengyu Huang − *Henan Key Laboratory of Nanomedicine for Targeting Diagnosis and Treatment, School of Pharmaceutical Sciences, Zhengzhou University, Zhengzhou 450001, China*

Jie Duan − *Henan Key Laboratory of Nanomedicine for Targeting Diagnosis and Treatment, School of Pharmaceutical Sciences, Zhengzhou University, Zhengzhou 450001, China*

Yue Qiu − *Henan Key Laboratory of Nanomedicine for Targeting Diagnosis and Treatment, School of Pharmaceutical Sciences, Zhengzhou University, Zhengzhou 450001, China*

Hua Yi − *Henan Key Laboratory of Nanomedicine for Targeting Diagnosis and Treatment, School of Pharmaceutical Sciences, Zhengzhou University, Zhengzhou 450001, China*

Yang Wang − *Henan Key Laboratory of Nanomedicine for Targeting Diagnosis and Treatment, School of Pharmaceutical Sciences, Zhengzhou University, Zhengzhou 450001, China*

Huimin Xue − *Henan Key Laboratory of Nanomedicine for Targeting Diagnosis and Treatment, School of Pharmaceutical Sciences, Zhengzhou University, Zhengzhou 450001, China*

Jiali Zhang − *Henan Key Laboratory of Nanomedicine for Targeting Diagnosis and Treatment, School of Pharmaceutical Sciences, Zhengzhou University, Zhengzhou 450001, China*

Qiuxia Yang − *Tianjian Laboratory of Advanced Biomedical Sciences, Zhengzhou University, Henan 450001, China*

Complete contact information is available at: https://pubs.acs.org/10.1021/acsami.4c09835

Author Contributions

†D.W. and X.Z. contributed equally to this work.

Notes

The authors declare no competing financial interest.

■ ACKNOWLEDGMENTS

This project is supported by the National Natural Science Foundation of China (Grants 22122409 and 22377110 to K.Z.), Henan Province Fund for Cultivating Advantageous Disciplines (No. 222301420019 to K.Z.), Key Scientific Research Projects (Science and Technology Department of Henan Province, No. 242102310080 to Z.G.), and Natural Science Foundation of Henan Province (No. 242300421125 to Q.Y.). All of the animal experiments were performed in accordance with the guidelines of the Regional Ethics Committee for Animal Experiments and Zhengzhou University Institutional Animal Care and Use Committee.

■ REFERENCES

(1) Li, M.; Jiang, H.; Hu, P.; Shi, J. Nanocatalytic Anti-Tumor Immune Regulation. *Angew. Chem., Int. Ed.* **2024**, *63*, No. e202316606.

(2) Yang, D.; Tang, Y.; Zhu, B.; Pang, H.; Rong, X.; Gao, Y.; Du, F.; Cheng, C.; Qiu, L.; Ma, L. Engineering Cell Membrane-Cloaked Catalysts as Multifaceted Artificial Peroxisomes for Biomedical Applications. *Adv. Sci.* **2023**, *10*, 2206181.

(3) Walsh, G. Biopharmaceutical Benchmarks 2018. *Nat. Biotechnol.* **2018**, *36*, 1136.

(4) Yu, Y.; Zhao, X.; Xu, X.; Cai, C.; Tang, X.; Zhang, Q.; Zhong, L.; Zhou, F.; Yang, D.; Zhu, Z. Rational Design of Orally Administered Cascade Nanozyme for Inflammatory Bowel Disease Therapy. *Adv. Mater.* **2023**, *35*, 2304967.

(5) Urquhart, L. Top Drugs and Companies by Sales in 2018. *Nat. Rev. Drug Discovery* **2019**, *18*, 245.

(6) Huang, J.; Xiao, Z.; Lin, M.; Zhong, H.; Shuai, X. Metal-organic framework nanoparticles hitchhiking on T cells for protein delivery to boost anticancer immunotherapy. *Nano Today* **2024**, *54*, 102102.

(7) Simó, C.; Serra-Casablancas, M.; Hortelao, A. C.; Di Carlo, V.; Guallar-Garrido, S.; Plaza-García, S.; Rabanal, R. M.; Ramos-Cabrer, P.; Aguado; Yagüe, L.; Bardia, L.; Tosi, S.; Gómez-Vallejo, V.; Martín, A.; Patiño, T.; Julián, E.; Colombelli, J.; Llop, J.; Sánchez, S. Urease-

powered nanobots for radionuclide bladder cancer therapy. *Nat. Nanotechnol.* **2024**, *19*, 554−564.
(8) Zhao, M.; Cheng, X.; Shao, P.; Dong, Y.; Wu, Y.; Xiao, L.; Cui, Z.; Sun, X.; Gao, C.; Chen, J.; Huang, Z.; Zhang, J. Bacterial protoplast-derived nanovesicles carrying CRISPR-Cas9 tools re-educate tumor-associated macrophages for enhanced cancer immunotherapy. *Nat. Commun.* **2024**, *15*, 950.
(9) Harris, J. M.; Chess, R. B. Effect of Pegylation on Pharmaceuticals. *Nat. Rev. Drug Discovery* **2003**, *2*, 214.
(10) Liu, X.; Gao, W. Precision Conjugation: An Emerging Tool for Generating Protein-Polymer Conjugates. *Angew. Chem., Int. Ed.* **2021**, *60*, 11024.
(11) Kontos, S.; Hubbell, J. A. Drug Development: Longer-Lived Proteins. *Chem. Soc. Rev.* **2012**, *41*, 2686.
(12) Wang, R.; Yu, Y.; Gai, M.; Maroto, A. M.; Morsbach, S.; Xia, X.; He, M.; Fan, J.; Peng, X.; Landfester, K.; Jiang, S.; Sun, W. Liposomal Enzyme Nanoreactors Based on Nanoconfinement for Efficient Antitumor Therapy. *Angew. Chem., Int. Ed.* **2023**, *135*, No. e202308761.
(13) Shi, Y.; Zhang, Y.; Zhu, L.; Miao, Y.; Zhu, Y.; Yue, B. Tailored Drug Delivery Platforms: Stimulus-Responsive Core-Shell Structured Nanocarriers. *Adv. Healthcare Mater.* **2024**, *13*, 2301726.
(14) Zhou, G.; Li, M. Near-Infrared-II Plasmonic Trienzyme-Integrated Metal-Organic Frameworks with High-Efficiency Enzyme Cascades for Synergistic Trimodal Oncotherapy. *Adv. Mater.* **2022**, *34*, 2200871.
(15) Peng, J.; Zhou, J.; Liu, X.; Zhang, X.; Zhou, X.; Gong, Z.; Chen, Y.; Shen, X.; Chen, Y. A Biomimetic Nanocarrier Facilitates Glucose Consumption and Reactive Oxide Species Accumulation in Enzyme Therapy for Colorectal Cancer. *J. Controlled Release* **2024**, *367*, 76−92.
(16) Shapir Itai, Y.; Barboy, O.; Salomon, R.; Bercovich, A.; Xie, K.; Winter, E.; Shami, T.; Porat, Z.; Erez, N.; Tanay, A.; Amit, I.; Dahan, R. Bispecific Dendritic-T Cell Engager Potentiates Antitumor Immunity. *Cell* **2024**, *187*, 375−389.
(17) Zhang, B.; Brahma, R. K.; Zhu, L.; Feng, J.; Hu, S.; Qian, L.; Du, S.; Yao, S. Q.; Ge, J. Insulin-like Growth Factor 2 (IGF2)-Fused Lysosomal Targeting Chimeras for Degradation of Extracellular and Membrane Proteins. *J. Am. Chem. Soc.* **2023**, *145*, 24272−24283.
(18) Siboro, P. Y.; Sharma, A. K.; Lai, P. J.; Jayakumar, J.; Mi, F. L.; Chen, H. L.; Chang, Y.; Sung, H. W. Harnessing HfO_2 Nanoparticles for Wearable Tumor Monitoring and Sonodynamic Therapy in Advancing Cancer Care. *ACS Nano* **2024**, *18*, 2485−2499.
(19) Wang, D.; Liu, J.; Duan, J.; Yi, H.; Liu, J.; Song, H.; Zhang, Z.; Shi, J.; Zhang, K. Enrichment and Sensing Tumor Cells by Embedded Immunomodulatory DNA Hydrogel to Inhibit Postoperative Tumor Recurrence. *Nat. Commun.* **2023**, *14*, 4511.
(20) Wang, F.; Xie, M.; Huang, Y.; Liu, Y.; Liu, X.; Zhu, L.; Zhu, X.; Guo, Y.; Zhang, C. In Situ Vaccination with An Injectable Nucleic Acid Hydrogel for Synergistic Cancer Immunotherapy. *Angew. Chem., Int. Ed.* **2024**, *63*, No. e202315282.
(21) Wang, B.; Chen, J.; Caserto, J. S.; Wang, X.; Ma, M. An in Situ Hydrogel-Mediated Chemo-immunometabolic Cancer Therapy. *Nat. Commun.* **2022**, *13*, 3821.
(22) Vora, L. K.; Sabri, A. H.; McKenna, P. E.; Himawan, A.; Hutton, A. R. J.; Detamornrat, U.; Paredes, A. J.; Larrañeta, E.; Donnelly, R. F. Microneedle-Based Biosensing. *Nat. Rev. Bioeng.* **2024**, *2*, 64−81.
(23) Zheng, M.; Sheng, T.; Yu, J.; Gu, Z.; Xu, C. Microneedle Biomedical Devices. *Nat. Rev. Bioeng.* **2024**, *2*, 324−342.
(24) Vivier, E.; Rebuffet, L.; NArni-Mancinelli, E.; Cornen, S.; Igarashi, R. Y.; Fantin, V. R. Natural Killer Cell Therapies. *Nature* **2024**, *626*, 727−736.
(25) Locke, F. L.; Filosto, S.; Chou, J.; Vardhanabhuti, S.; Perbost, R.; Dreger, P.; Hill, B. T.; Lee, C.; Zinzani, P. L.; Kröger, N.; López-Guillermo, A.; Greinix, H.; Zhang, W.; Tiwari, G. J.; Budka, F. M.; Marincola, C.; To, M.; Mattie, M.; Schupp, P.; Cheng, A.; Bot, R.; Shen; Bedognetti, D.; Miao, H.; Galon, J. Impact of Tumor Microenvironment on Efficacy of Anti-CD19 CAR T Cell Therapy or Chemotherapy and Transplant in Large B Cell Lymphoma. *Nat. Med.* **2024**, *30*, 507−518.
(26) Vincent, R. L.; Gurbatri, C. R.; Li, F.; Vardoshvili, A.; Coker, C.; Im, J.; Ballister, E. R.; Rouanne, M.; Savage, T.; de los Santos-Alexis, K.; Redenti, A.; Brockmann, L.; Komaranchath, M.; Arpaia, N.; Danino, T. Probiotic-Guided CAR-T Cells for Solid Tumor Targeting. *Science* **2023**, *382*, 211−218.
(27) Zhong, Y.; Xu, L.; Yang, C.; Xu, L.; Wang, G.; Guo, Y.; Cheng, S.; Tian, X.; Wang, C.; Xie, R.; Wang, X.; Ding, L.; Ju, H. Site-Selected in Situ Polymerization for Living Cell Surface Engineering. *Nat. Commun.* **2023**, *14*, 7285.
(28) Han, J.; Bhatta, R.; Liu, Y.; Bo, Y.; Elosegui-Artola, A.; Wang, H. Metabolic Glycan Labeling Immobilizes Dendritic Cell Membrane and Enhances Antitumor Efficacy of Dendritic Cell Vaccine. *Nat. Commun.* **2023**, *14*, 5049.
(29) Wu, Y.; Lin, B.; Lu, Y.; Li, L.; Deng, K.; Zhang, S.; Zhang, H.; Yang, C.; Zhu, Z. Aptamer-LYTACs for Targeted Degradation of Extracellular and Membrane Proteins. *Angew. Chem., Int. Ed.* **2023**, *62*, No. e202218106.
(30) Tian, Y.; Miao, Y.; Guo, P.; Wang, J.; Han, D. Insulin-like Growth Factor 2-Tagged Aptamer Chimeras (ITACs) Modular Assembly for Targeted and Efficient Degradation of Two Membrane Proteins. *Angew. Chem., Int. Ed.* **2024**, *63*, No. e202316089.
(31) Qian, L.; Lin, X.; Gao, X.; Khan, R. U.; Liao, J. Y.; Du, S.; Ge, J.; Zeng, S.; Yao, S. Q. The Dawn of a New Era: Targeting the "Undruggables" with Antibody-Based Therapeutics. *Chem. Rev.* **2023**, *123*, 7782−7853.
(32) Zhu, C.; Wang, W.; Wang, Y.; Zhang, Y.; Li, J. Dendronized DNA Chimeras Harness Scavenger Receptors to Degrade Cell Membrane Proteins. *Angew. Chem.* **2023**, *135*, No. e202300694.
(33) Pance, K.; Gramespacher, J. A.; Byrnes, J. R.; Salangsang, F.; Serrano, J. A. C.; Cotton, A. D.; Steri, V.; Wells, J. A. Modular Cytokine Receptor-Targeting Chimeras for Targeted Degradation of Cell Surface and Extracellular Proteins. *Nat. Biotechnol.* **2023**, *41*, 273−281.
(34) Zhang, A. Q.; Hostetler, A.; Chen, L. E.; Mukkamala, V.; Abraham, W.; Padilla, L. T.; Wolff, A. N.; Maiorino, L.; Backlund, C. M.; Aung, A.; Melo, M.; Li, N.; Wu, S.; Irvine, D. J. Universal Redirection of CAR T Cells Against Solid Tumours via Membrane-Inserted Ligands for the CAR. *Nat. Biomed. Eng.* **2023**, *7*, 1113−1128.
(35) Du, Y.; Lyu, Y.; Lin, J.; Ma, C.; Zhang, Q.; Zhang, Y.; Qiu, L.; Tan, W. Membrane-Anchored DNA Nanojunctions Enable Closer Antigen-Presenting Cell-T-cell Contact in Elevated T-cell Receptor Triggering. *Nat. Nanotechnol.* **2023**, *18*, 818−827.
(36) Yin, Y.; Xie, W.; Xiong, M.; Gao, Y.; Liu, Q.; Han, D.; Ke, G.; Zhang, X. B. A Fluidly Confined CRISPR-Based DNA Reporter on Living Cell Membranes for Rapid and Sensitive Cancer Cell Identification. *Angew. Chem., Int. Ed.* **2023**, *62*, No. e202309837.
(37) Yang, Q.; Guo, Z.; Liu, H.; Peng, R.; Xu, L.; Bi, C.; He, Y.; Liu, Q.; Tan, W. A Cascade Signaling Network between Artificial Cells Switching Activity of Synthetic Transmembrane Channels. *J. Am. Chem. Soc.* **2021**, *143*, 232−240.
(38) Ye, T.; Liu, X.; Zhong, X.; Yan, R.; Shi, P. Nongenetic Surface Engineering of Mesenchymal Stromal Cells with Polyvalent Antibodies to Enhance Targeting Efficiency. *Nat. Commun.* **2023**, *14*, 5806.
(39) Guo, Z.; Zhang, L.; Yang, Q.; Peng, R.; Yuan, X.; Xu, L.; Wang, Z.; Chen, F.; Huang, H.; Liu, Q.; Tan, W. Manipulation of Multiple Cell-Cell Interactions by Tunable DNA Scaffold Networks. *Angew. Chem., Int. Ed.* **2022**, *61*, No. e202111151.

https://doi.org/10.1021/acsami.4c09835
ACS Appl. Mater. Interfaces 2024, 16, 50295−50304